

Neuronal Excitability

Intrinsic Sources and Functional Impacts of Asymmetry at Electrical Synapses

Austin J. Mendoza and Julie S. Haas

<https://doi.org/10.1523/ENEURO.0469-21.2022>

Department of Biological Sciences, Lehigh University, Bethlehem, PA 18015

Abstract

Electrical synapses couple inhibitory neurons across the brain, underlying a variety of functions that are modifiable by activity. Despite recent advances, many functions and contributions of electrical synapses within neural circuitry remain underappreciated. Among these are the sources and impacts of electrical synapse asymmetry. Using multi-compartmental models of neurons coupled through dendritic electrical synapses, we investigated intrinsic factors that contribute to effective synaptic asymmetry and that result in modulation of spike timing and synchrony between coupled cells. We show that electrical synapse location along a dendrite, input resistance, internal dendritic resistance, or directional conduction of the electrical synapse itself each alter asymmetry as measured by coupling between cell somas. Conversely, we note that asymmetrical gap junction (GJ) conductance can be masked by each of these properties. Furthermore, we show that asymmetry modulates spike timing and latency of coupled cells by up to tens of milliseconds, depending on direction of conduction or dendritic location of the electrical synapse. Coordination of rhythmic activity between two cells also depends on asymmetry. These simulations illustrate that causes of asymmetry are diverse, may not be apparent in somatic measurements of electrical coupling, influence dendritic processing, and produce a variety of outcomes on spiking and synchrony of coupled cells. Our findings highlight aspects of electrical synapses that should always be included in experimental demonstrations of coupling, and when assembling simulated networks containing electrical synapses.

Key words: asymmetry; computational model; electrical synapse; gap junction; rectification

Significance Statement

Asymmetry, or unequal transmission of current between two coupled neurons, is a property of electrical synapses often noted but seldom explored. Here, we show that multiple intrinsic factors can either produce, or mask, asymmetry. Spike timing and rhythmic synchrony are both affected by asymmetric connections between neurons. These results highlight important consequences of asymmetry that are likely to be recapitulated within coupled networks throughout the brain.

Introduction

Electrical synapses represent a major form of communication between neurons across neuronal tissue, with many impacts that have not been extensively explored. Asymmetry of transmission, is a frequently noted aspect of electrical synapses: it is the property of unequal transmission of electrical signals between two neurons, and ranges in effect from minor to complete. Electrical

synapses have been well studied in invertebrates, where evidence of asymmetry comes from species including crayfish (Furshpan and Potter, 1959), *Drosophila* giant fibers (Phelan et al., 2008), lobster stomatogastric ganglion (Johnson et al., 1993), and the *Caenorhabditis elegans* escape circuit (Liu et al., 2017; Shui et al., 2020). In invertebrate systems, asymmetry varies widely, with some synapses displaying full rectification. In contrast, asymmetry at synapses between mammalian neurons is often

Received November 3, 2021; accepted February 2, 2022; First published February 8, 2022.

The authors declare no competing financial interests.

Author contributions: A.J.M. and J.S.H. designed research; A.J.M. performed research; A.J.M. analyzed data; A.J.M. and J.S.H. wrote the paper.

more modest. Demonstrations of electrical synapse asymmetry are numerous throughout the mammalian brain, including retina (Veruki and Hartveit, 2002), cortex (Galarreta and Hestrin, 2002), inferior olive (Devor and Yarom, 2002), dorsal cochlear nucleus (Apostolides and Trussell, 2013), mesencephalic trigeminal nucleus (Curti et al., 2012), cerebellar Golgi cells (Szoboszlay et al., 2016) and molecular layer interneurons (Mann-Metzer and Yarom, 1999; Alcami and Marty, 2013), and the thalamic reticular nucleus (TRN; Haas et al., 2011; Sevetson and Haas, 2015; Zolnik and Connors, 2016). Recent results show that asymmetry can be modified during the activity that results in electrical synapse plasticity (Haas et al., 2011; Fricker et al., 2021), indicating that it is a dynamic property that is under activity-dependent regulation.

Asymmetry of electrical transmission can in principle result from a wide variety of influences. It has been well established in non-mammalian systems that directional differences in conductance between two coupled cells can result from heteromeric channels or heterotypic gap junction (GJ) plaques that coupled membranes (Bukauskas et al., 1995; Rash et al., 2013), or from differences in hemichannel protein scaffolding (Marsh et al., 2017). Hemichannel differences resulting in asymmetry have been demonstrated in HeLa cells expressing connexin isoforms (Bukauskas et al., 1995) and at the mixed synapse onto Mauthner cells in goldfish (Rash et al., 2013). Connexin-sourced asymmetry was thought to be unlikely for neuronal mammal synapses, as connexin36 does not oligomerize or dock with other connexins (Teubner et al., 2000; Li et al., 2004), and in expression systems appears to form perfectly symmetric synapses (Srinivas et al., 1999). However, residual coupling has been noted between TRN neurons in connexin36 knock-out mice, and that coupling was more asymmetrical (Zolnik and Connors, 2016), indicating a possible physiological source of synaptic asymmetry in mammalian neuronal systems. Large gradients of Mg^{2+} concentration produce asymmetric signaling for neuronal synapses (Palacios-Prado et al., 2013), and gating properties of connexin channels produce asymmetry in computational models (Snipas et al., 2017). Cable properties of coupled dendrites affect voltage transmission (Nadim and Golowasch, 2006), indicating that differences in dendritic diameter may produce asymmetric coupling. Intrinsic differences between coupled neurons, such as differences in input resistance (Bennett, 1966; Mann-Metzer and Yarom, 1999; Veruki and Hartveit, 2002; Fortier, 2010) or leak conductances (Alcami and

Marty, 2013), have long been mentioned as a straightforward reason that one might observe asymmetry in coupling coefficients. For TRN synapses, asymmetry remains even after computing estimates of conductance that should in principle minimize contributions of input resistance (Haas et al., 2011; Sevetson and Haas, 2015). And while many reports of electrical synapses across the mammalian brain include asymmetry in their measurements, some reports do not note it, or only note that in their observations, synapses were symmetrical as expected. In all, asymmetry and its sources remain underappreciated at mammalian electrical synapses.

Beyond observations, the functional consequences of electrical synapse asymmetry on neural activity are not robustly understood. Electrical synapses have been widely shown to contribute toward synchrony of rhythmic activity in neuronal networks in both experiments (Marder, 1998; Draguhn et al., 1998; Galarreta and Hestrin, 1999; Gibson et al., 1999; Mann-Metzer and Yarom, 1999; Tamás et al., 2000; Hormuzdi et al., 2001; Landisman et al., 2002; Blatow et al., 2003; Bennett and Zukin, 2004; Long, 2004; Christie et al., 2005; Long et al., 2005; Vervaeke et al., 2010) and in computational models (Kepler et al., 1990; Sherman and Rinzel, 1992; Destexhe et al., 1996; Manor et al., 1997; Skinner et al., 1999; Chow and Kopell, 2000; Lewis and Rinzel, 2003; Whittington and Traub, 2003; Kopell and Ermentrout, 2004; Nomura et al., 2004; Saraga and Skinner, 2004; Pfeuty et al., 2005; Traub et al., 2005; O'Connor et al., 2012; Gutierrez et al., 2013; Pernelle et al., 2018), and oscillations are more robust when asymmetrical electrical synapses are included (Gutierrez and Marder, 2013). Rectification at the LP-PY mixed synapse is a key component of coordinating the pyloric circuit of the spiny lobster (Mamiya et al., 2003). In non-rhythmic settings, strong asymmetry can produce nearly unidirectional communication that serves to reliably excite one coupled cell, as is the case with the club endings onto Mauthner cells in goldfish (Rash et al., 2013), and dorsal cochlear nucleus (Apostolides and Trussell, 2013). Electrical synapses modulate individual spike times in coupled neighbors in TRN by up to tens of milliseconds (Haas, 2015; Sevetson and Haas, 2015), and asymmetric coupling can add to that modulation, even reversing firing order between two coupled cells that receive closely-timed inputs (Sevetson and Haas, 2015). In a model thalamocortical circuit, coupling between feedback inhibitory neurons enhances discrimination of inputs sent to cortex by relay cells (Pham and Haas, 2018). In a canonical model circuit with feedforward inhibition, electrical synapses enhance subthreshold integration in principal cells (Pham and Haas, 2019). In a toadfish vocal circuit, electrical coupling between feedforward inhibitory neurons enhances synchrony and temporal precision (Chagnaud et al., 2021) and a similar effect occurs for cerebellar basket cells (Alcami, 2018; Hoehne et al., 2020). These are some of the functions that could be altered by asymmetry. While a few models have included electrical synapses in morphologically extended cells (Saraga and Skinner, 2004; Nadim and Golowasch, 2006; Amsalem et al.,

This work was supported by the National Science Foundation Grant IOS 1557474.

Acknowledgements: We thank Mitchell Vaughn, Meghan Bauer, and Zachary Laswick for input on drafts of this manuscript.

Correspondence should be addressed to Julie S. Haas at julie.haas@lehigh.edu.

<https://doi.org/10.1523/ENEURO.0469-21.2022>

Copyright © 2022 Mendoza and Haas

This is an open-access article distributed under the terms of the Creative Commons Attribution 4.0 International license, which permits unrestricted use, distribution and reproduction in any medium provided that the original work is properly attributed.

2016), the sources or functions of asymmetrical synapses have not yet been explored in that context.

Here, we used compartmental models of coupled TRN neurons to investigate and compare how a variety of fundamental neuronal properties could each contribute to electrical synapse asymmetry, including synapse location, strength, direction of conductance, dendritic geometry, and input resistance. We show that, as predicted, a variety of these factors can produce effective differences in coupling coefficients as observed between somas. We then demonstrate that conversely, these same properties can mask asymmetric conductance of electrical synapses, resulting in apparently equal coupling as measured between somas. Together, these results underline that asymmetric transmission and impacts are likely to occur more widely than previously considered. Finally, we show that asymmetry regulates spike timing and, unexpectedly, the form of rhythmic coordination in coupled neurons. We conclude that electrical synapses between dendrites can exert locally powerful influence that is not readily apparent at the soma, highlighting the necessity of including electrical synapses in morphologically detailed models, circuits or connectomes.

Materials and Methods

Modelling

Models were built on those previously reported (Destexhe et al., 1996; Traub et al., 2005; Haas and Landisman, 2012; Pham and Haas, 2018, 2019). We use Hodgkin–Huxley formalism (Eq. 1) solved by a second order Runge–Kutta ODE solver in MATLAB version R2020b (MathWorks), simulations were run on an ASUS desktop PC with Intel i7-10700K CPU running Windows 10:

$$C_m \frac{dV_i}{dt} = G_{leak} \cdot (E_{leak} - V_i) + \sum_{\substack{\text{ion} \\ \text{channels}}} G_{ion}(t) \cdot (E_{ion} - V_i) + \sum_{\substack{j \neq i \\ \text{chemical} \\ \text{synapses}}} G_{syn} \left(t, t_j^{events} \right) \cdot (E_{syn} - V_i) + \sum_{\substack{j \neq i \\ \text{electrical} \\ \text{synapses}}} G_{elec\,ji} \cdot (V_j - V_i) + \sum_{\substack{\text{external} \\ \text{inputs}}} G_{syn} \left(t, t_{external}^{events} \right) \cdot (E_{syn} - V_i) + \sum_{\substack{j \neq i \\ \text{coupled} \\ \text{compartments}}} G_{internal\,ji} \cdot (V_j - V_i) \quad (1)$$

The single compartment TRN cell model included the following ionic currents and maximal conductances: fast transient Na⁺ (Na_T) 60.5 mS/cm², K⁺ delayed rectifier (K_d) 60 mS/cm², K⁺ transient A (K_t) 5 mS/cm², slowly inactivating K⁺ (K₂) 0.5 mS/cm², slow anomalous rectifier (AR) 0.025 mS/cm², and low threshold transient Ca²⁺ (Ca_T) 0.75 mS/cm². Reversal potentials were 50 mV for sodium, −100 mV for potassium, 125 mV for calcium, −40 mV for AR and −75 mV for leak. Capacitance was 1 μF/cm² with leak of 0.1 mS/cm². Three-compartment models were constructed consisting of one soma and two dendritic compartments, approximating the middle and distal

regions of the dendrite. Compartments were connected by a static conductance G_{internal} of 0.35 mS/cm² between distal and middle dendrites, and 0.4 mS/cm² between middle dendrite and soma. Membrane capacitance was 1.2 μF/cm². Maximal conductance for the compartmental model were: Na_T 60.5 mS/cm², K_d 90 mS/cm², K_t 5 mS/cm², K₂ 0.5 mS/cm², AR 0.005 mS/cm², and Ca_T 0.5 mS/cm². Leak conductance was set at 0.1 mS/cm² for soma compartments, and 0.035 mS/cm² for dendrites, except when altering input resistance where leak conductance was scaled by 0.75–1.45 times, corresponding to ±25% change in input resistance. Dendritic compartments had lower Ca_T conductance of 0.15 mS/cm². We removed the sodium current from dendrites, as TRN dendrites do not spike in recordings (Connelly et al., 2017). Electrical synapses were modeled as a static conductance G_{elec} (referred to as G_c in Results) applied to the voltage difference between the coupled compartments of the TRN cells. Asymmetry was implemented by varying G_{elec} for each cell. Excitatory synapses were AMPAergic with reversal potential of 0 mV with rise and fall time kinetics of 5 ms and 35 ms respectively.

Analysis

Coupling coefficients were measured by injecting hyperpolarizing current into the soma of one cell (A) and measuring the resulting current deflection in the soma of the other cell (B) compared with baseline (CC_{AB} = ΔV_B/ΔV_A), matching experimental methodology. We used 500-ms-long square current injection and measured coupling in both directions between the cell pairs. The steady-state voltage during hyperpolarization was taken as the average voltage during the last 200 ms of stimulation. Coupling coefficient ratio was calculated as CC₁₂/CC₂₁.

To analyze latency modulation produced by electrical synapses we applied burst like EPSCs to distal dendrites of the model TRN cells and measured the time between onset of the first EPSC to the first action potential. Bursts consisted of 13 EPSCs of 1-μA amplitude with 5-ms interspike interval (ISI), 0.5-μA depolarizing current was applied to raise excitability of the cell model. Latency modulation was expressed as the difference in the change of latency between the two cells, compared with the latency of an uncoupled model cell. Synchrony was examined using single cell models driven to spike tonically, with one cell driven slightly higher, I₁ = 0.575, I₂ = 0.6 μA/cm². Cross-correlations were taken for a 500-ms time window during stable tonic firing, spike trains were filtered with a 5-ms Hanning window. Time lag values from the peak of the cross correlations were taken to calculate phase difference between the two spike trains (phase difference = t_{max lag}/ISI × 360). To examine the effect of asymmetry, coupling was constant in the cell 2–1 direction and scaled coupling in the 1–2 direction to obtain ratios between 0.3 and 3 times, the range observed from paired recordings at TRN.

Code availability

The code/software described in the paper is freely available online at <https://github.com/jhaaslab/Asymmetry>. The code is also available as [Extended Data 1](#).

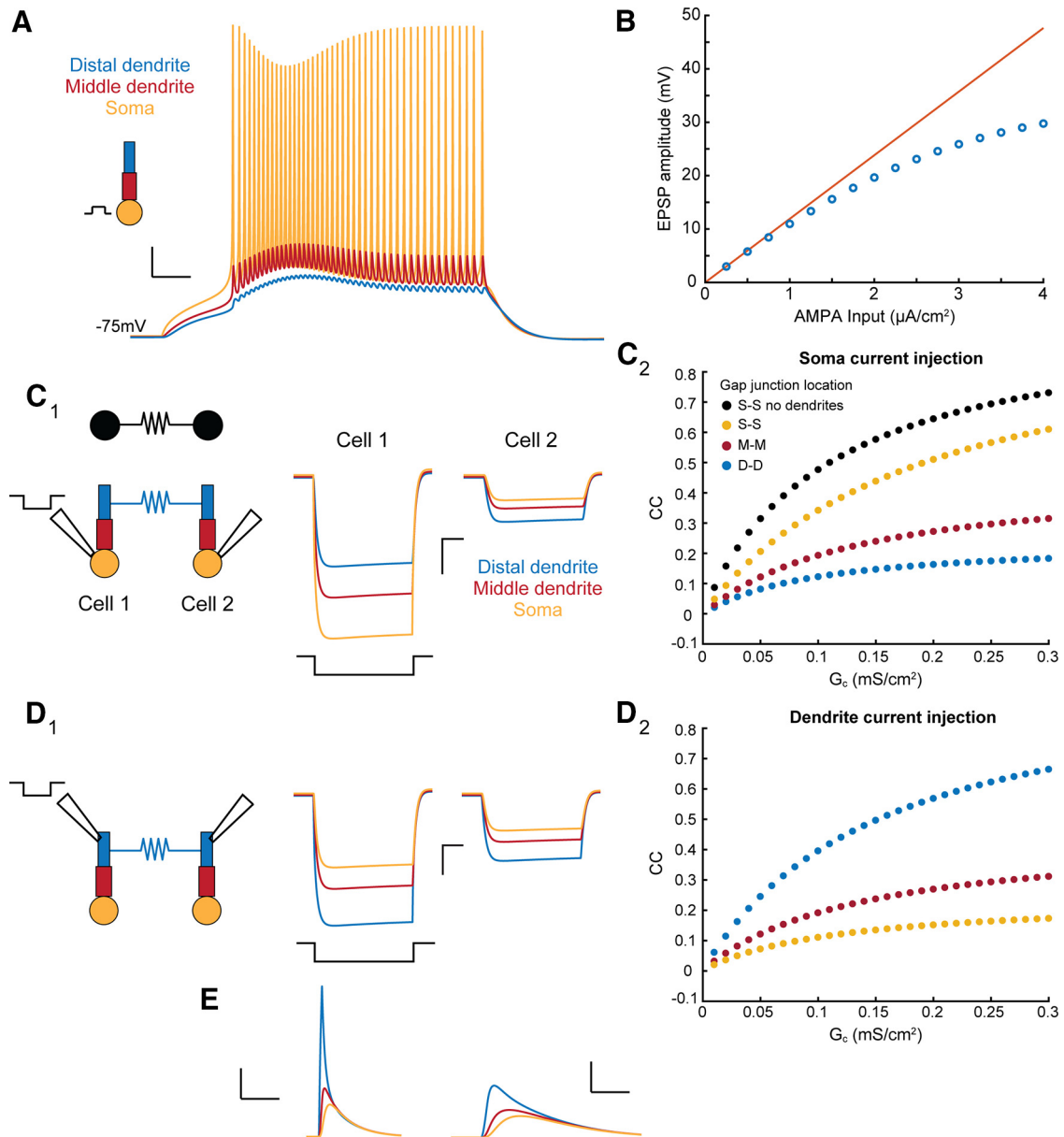


Figure 1. Compartmental TRN model and characterization of coupling responses for GJs at varied dendritic locations. **A**, Schematic of compartmental TRN model and representative traces from each compartment in response to square depolarizing current injection at the soma compartment. Scale bars: 10 mV, 25 ms. **B**, Postsynaptic response to an AMPAergic input delivered to distal dendrite. EPSP amplitudes were sublinear above $2\ \mu\text{A}$, due to lack of active conductances in dendrites. **C₁**, Schematic for electrically coupled models. Voltage traces in both cells result from a hyperpolarizing current injection into the soma of cell 1 (left traces) and transfer to cell 2 (right traces). Scale bars: 5 mV, 100 ms. **C₂**, Coupling coefficients (cc) measured between somatic compartments as in **C₁** for GJs located between the somas (yellow), middle compartments (red), and distal dendrites (blue). An identical single-compartment model is shown for comparison (black). **D₁**, Schematic and voltage traces for coupling measured between dendrites after dendritic current injection. **D₂**, Coupling coefficients (cc) measured between dendritic compartments as in **D₁** for GJs located between the somas (yellow), middle compartments (red), and distal dendrites (blue). **E**, EPSP amplitudes for each compartment for distally applied EPSC to cell 1 (left traces; scale bars: 2 mV, 25 ms), transmitted to cell 2 across a distal electrical synapse (right traces; scale bars: 1 mV, 12.5 ms).

Results

To address the impact of neuronal excitability and morphology on electrical synapse communication, we built a three-compartment TRN cell Hodgkin–Huxley model, including a T-type calcium conductance in addition to leak, sodium, and potassium conductances, based on those

previously used (Destexhe et al., 1996; Traub et al., 2005; Pham and Haas, 2018, 2019). To validate the model’s dendritic responses, we used coupling between compartments that generated reasonable amplitudes of backpropagated signals (Fig. 1A), sublinear dendritic responses to AMPAergic current injections (Fig. 1B) that matched

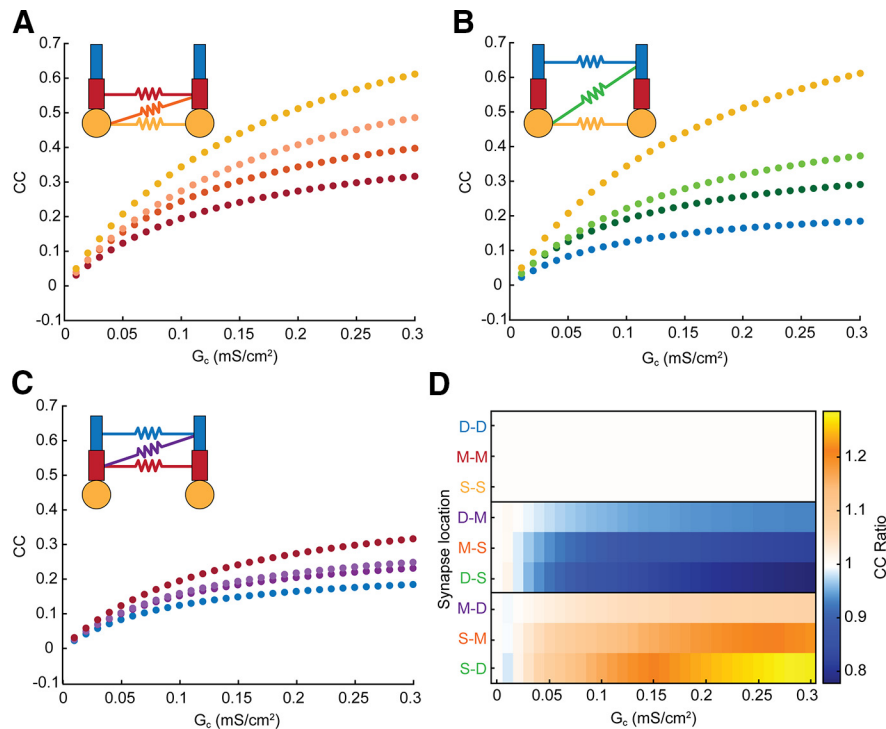


Figure 2. Electrical synapse location and strength contribute to coupling coefficient and asymmetry measured at the soma. **A**, Coupling coefficients measured from cell 1 to cell 2 for all sets of somatic and middle-compartment electrical synapses. Soma-soma synapses are in yellow, middle-middle synapses are in red, and both types of soma-middle synapses are orange with opposite coupling (M-S) indicated by darker shaded datapoints. **B**, As in **A** for somatic and distal synapse locations. **C**, As in **A** for middle and distal synapse locations; note overall decrease in coupling for more-distant synapses. **D**, Coupling coefficient ratio (cc_{12}/cc_{21}) for each synapse location and strength. Locations are grouped by effect; the top box shows GJs between matched compartments that are symmetric, as expected. In the middle box, the GJ was closer to the soma of cell 2, and thus cc_{21} was larger. In the bottom box, the GJ was closer to the soma of cell 1, and thus cc_{12} was larger. Asymmetry increased with difference between location of the GJ, and with proximity to the soma.

dendritic recordings from TRN cells (Connelly et al., 2017) and firing responses from our own recordings (Haas et al., 2011; Severson and Haas, 2015). We then added an electrical synapse between matched compartments of two identical TRN model cells and measured the coupling coefficients resulting from hyperpolarizing current applied to and measured at the somas (Fig. 1C1). We chose coupling conductance values to match coupling coefficients observed in recordings, cc between 0 and 0.3 (Haas et al., 2011). For these matched-compartment connections, electrical synapses produced higher coupling coefficients when synapses were closer to the soma, as the current between electrodes has a more direct path (Fig. 1D1). A single-compartmental model used for comparison (Fig. 1C1,D1, black) resulted in stronger coupling coefficients, as removing dendrites reduced leaks from the circuit. Similarly, when current is applied and coupling measurements are taken between distal dendrites (Fig. 1C2), coupling is stronger at dendritically located synapses but decreases as the synapse location approaches the soma (Fig. 1D2). This is a simple result of cable properties, but highlights the notion that electrical synapses can produce strong and effective coupling between dendritic compartments (Fig. 1E) that is not apparent from somatic measurements.

Next, we varied the location of electrical synapses between the dendritic compartments of each cell, and again

measured coupling between somas of cell 1 and cell 2. In all cases, the coupling for mixed-location synapses was intermediate to the values obtained for connections between matched compartments (Fig. 2A–C). Interestingly, coupling values for pairs of compartment connections that one might initially expect to produce the same coupling, such as soma-middle (S-M) and middle-soma (M-S; Fig. 2A, orange dots), do not produce identical coupling coefficients. The source of asymmetry in this case is the differences in dendritic leaks that siphon soma-applied current from the GJ pathway. Specifically, for S-M connections, the dendritic load for soma-applied current comprises resistance from both M and D compartments and is larger than the remaining dendritic leak from a single D compartment when current is applied to the opposite soma. These differences lead to differences in the currents crossing the GJ when current is separately applied to each soma, and thus the coupling coefficients are asymmetric as measured between somas. Comparing Figure 2A–C, we note that this effect is strongest for connections closer to the soma, where the differences in dendrites distal to the electrical synapse are largest.

We compared asymmetry, or cc ratios, for all synapse locations as a function of synapse strength (Fig. 2D). As expected, connections between the same compartments (e.g., M-M) were perfectly symmetrical for all values of

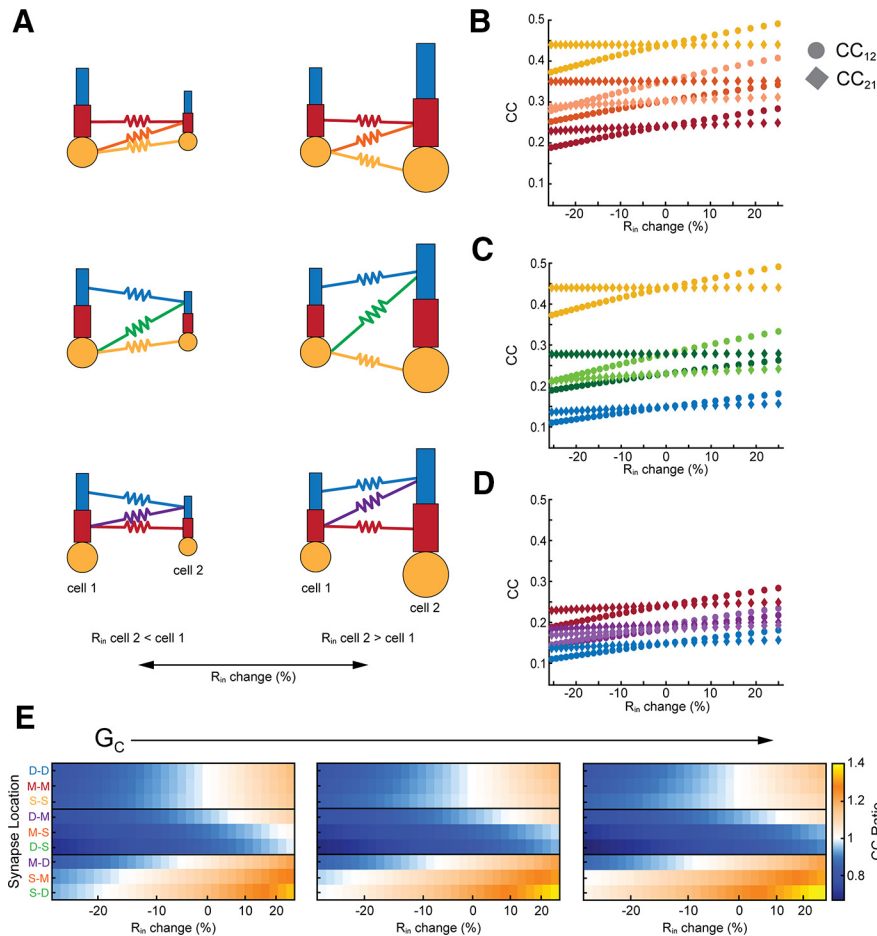


Figure 3. Dependence of asymmetry on synapse location and input resistance differences. **A**, Schematics depicting differences in input resistance, and varied synapse locations. **B**, Coupling versus difference in input resistance for GJs ($G_C = 0.15 \text{ mS/cm}^2$) between middle-middle, middle-soma, and soma-soma compartments. Difference in input resistance is expressed as cell 2 relative to cell 1. **C**, As in **B** for GJs between distal and soma compartments. **D**, As in **B** for GJs between distal and middle compartments. **E**, Asymmetry plotted against input resistance differences, grouped by electrical synapse strength (G_C), which increases across panels: 0.1, 0.15, and 0.2 mS/cm^2 .

electrical synapse conductance. In contrast, mismatched synapses are marked by decreasing or increasing cc ratios, with the mirror cases producing similar degrees of effective asymmetry in opposite directions (e.g., M-D and D-M). We also noted that asymmetry was greater for more-mismatched synapse pairs (e.g., S-D and M-D, or the blocks in Fig. 2D), as the distal-soma connections produce cc ratios furthest from 1. Further, asymmetry was greatest for synapses connected to the soma, while M-D synapses showed a lesser degree of effective asymmetry. These simulations demonstrate that effective asymmetry between somatic integrators can arise from difference in synapse location, when perfectly symmetrical electrical synapses encounter asymmetrical spatial differences between identical somas and dendrites, and thereby dictate effective asymmetry.

Effective asymmetry can also arise from differences in basic excitability, e.g., membrane input resistance R_{in} . To demonstrate this widely expected phenomenon, we altered R_{in} by changing leak conductance in cell 2 of the model (Fig. 3A), and measuring coupling coefficient cc in

both directions. When GJs coupled two somas of differing R_{in} , cc was determined only by R_{in} of cell 2 (Fig. 3B, yellow); cc_{12} varied, while cc_{21} stayed constant. As GJs were more distant from the soma, voltage divisions allowed both cc_{12} and cc_{21} to change, although changes in cc_{12} were always larger. Differences in GJ location also contributed to asymmetry here, again splitting the differences between the extremes, similarly to the effect shown in Figure 2.

The combined effects of input resistance and location are summarized in Figure 3E, which shows simulations for three values of average electrical synapse strength G_C for all synapse locations and input resistance mismatches. For matched-compartment locations (top boxes), asymmetry was determined only by differences in R_{in} . For GJs that coupled cells with differing R_{in} and synapses at mismatched locations, synapse location appeared to be a weaker effect than input resistance mismatch: the cell with the GJ closer to its soma always yielded a smaller coupling (e.g., middle box: synapses are closer to soma 2, and produced asymmetry < 1). As in Figure 2,

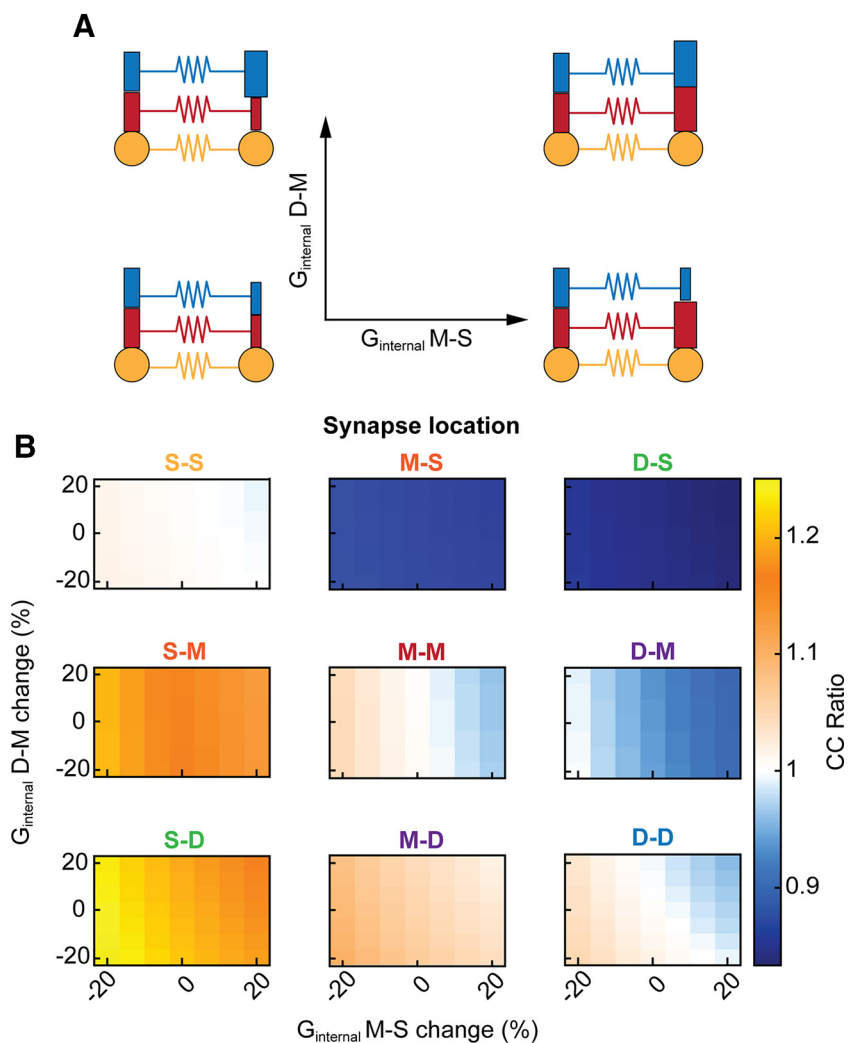


Figure 4. Differences in dendritic morphology fine-tune coupling coefficients and asymmetry. **A**, Internal conductances between the three subcellular compartments were altered in cell 2, as shown in schematics. Changes in middle-soma conductance is plotted on the x-axis, and change in distal-middle conductance is plotted on the y-axis. **B**, Heat maps of cc ratio for all synapse locations. In all cases, decreasing internal conductance increased cc ratio, while increasing internal conductance in decreased cc ratio. G_C was 0.15 mS/cm^2 for all synapses in these simulations.

asymmetry was strongest for synapses coupling the most spatially separate compartments. These simulations showed us that increasing G_C amplified the asymmetry produced by differences in R_{in} . Synapses that were mostly below one in cc ratio further decreased in cc ratio (Fig. 3E, middle rows), while locations with cc ratio above one increased with the strength of the synapse (Fig. 3E, bottom rows). Synapses between similar compartments (top rows) showed minimal changes with increasing strength of the synapse.

To further examine how heterogeneity between two coupled cells could contribute to effective asymmetry, we altered the internal coupling conductance between compartments of the cell. For all synapse locations, differences in dendritic coupling altered resulting cc ratios (Fig. 4), but by amounts smaller than synapse mismatch or input resistance difference. Increasing dendritic conductance favors transmission into that cell and thus

lowers cc ratio when cell 2 has more-conductive dendrites. Similarly, cc ratio increases when cell 1 is higher in dendritic conductance. This result is consistent for the connections between same cellular compartments, which are symmetric when morphology is the same, and the mismatched locations which are asymmetric in the same case. Although morphology may not produce substantial asymmetry alone, in conjunction with synapse location the intrinsic differences between two cells will fine-tune the overall coupling and asymmetry measured between them.

The previous sets of simulations used a symmetrical synapse to show that several aspects of cellular properties and synapse locations can yield effective asymmetry, as expected. Next, we asked whether an electrical synapse that was itself asymmetrical could produce the same effective asymmetries. We varied the conductance G_C of the electrical synapse between somatic

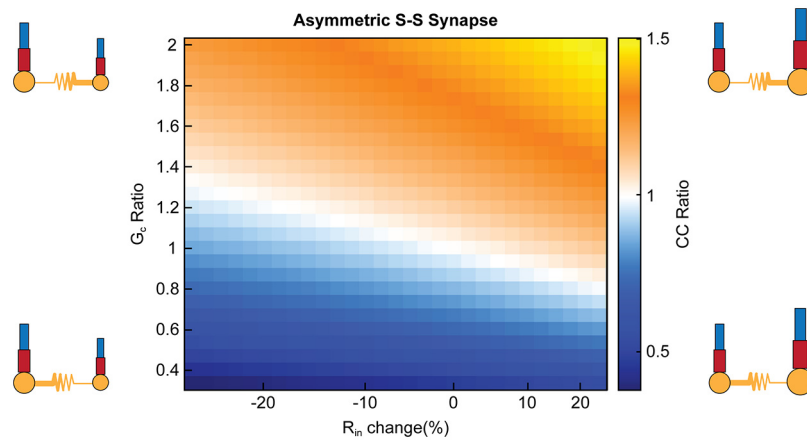


Figure 5. Asymmetry due to altering directional conductance produces similar response in coupling coefficients compared with synapse location asymmetry. Directional conductance changes between the cells produces a similar degree of asymmetry in cc ratio, with input resistance difference between the two cells predictably shifts the cc ratio values. G_c ratio (G_{c12}/G_{c21}) from altering conductance from cell 1 to cell 2 was varied, while the opposite direction was held constant ($G_{c21} = 0.15 \text{ mS/cm}^2$). Input resistance was altered in cell 2 relative to cell 1. Neuron schematics depict direction with larger conductance as a thicker resistor symbol, while size of the cell indicates change in input resistance.

compartments, and again examined the effect of input resistance changes on effective asymmetry. Our results demonstrate that similar values of effective asymmetry could arise from either G_c ratio or input resistance difference (Fig. 5). For each set of input resistances (Fig. 5, column), synaptic asymmetry could produce a range of effective asymmetry. These simulations illustrate the potential for cc values recorded from the soma to appear similarly asymmetric, whether asymmetry is produced from differential intrinsic properties or synapses themselves.

Together, the previous results show that asymmetry in coupling as measured between somas can arise from a number of factors. We demonstrate this masking in Figure 6 the same amount of asymmetry in coupling as measured at the soma can arise from independent sources. We identified simulations that resulted in 20% coupling difference, as this is the most common cc ratio observed in paired recordings at TRN (Haas et al., 2011). Higher transmission to cell 2 by the same proportion (cc ratio ~ 1.2) can be produced by asymmetric GJ with G_c ratio of 1.8 and R_{in} change of -20% (Fig. 6B), or M-D synapse location and $+25\%$ R_{in} change (Fig. 6D), or S-M synapse with higher dendritic conductance in cell 1 (Fig. 6F). Alternatively, higher transmission to cell 1 (cc ratio ~ 0.8) can be produced by asymmetric GJ with G_c ratio of 0.67 and $+6\%$ R_{in} change (Fig. 6C), or M-S synapse and -12% R_{in} change (Fig. 6E), or D-S synapse with higher dendritic conductance in cell 2 (Fig. 6G). Thus, asymmetry measured at the soma is not informative as to its source, and more pertinently, fails to provide insight into processing in coupled dendrites.

Next, we examined the impact of asymmetry on the function of coupled pairs. Electrical synapses have been previously shown to modulate latency of action potentials in coupled pairs (Haas, 2015; Severson and Haas, 2015; Alcami, 2018). We measured latency to burst-like input patterns of AMPAergic synaptic currents delivered to

distal dendrites of both cells of a coupled pair, to mimic excitatory afferent activity received by cells of the TRN (Gentet and Ulrich, 2003) from bursting thalamic relay cells (Fig. 7A). We tested each synapse location, and also varied the arrival (onset) times of the AMPAergic bursts between the two cells. For synapses between the similar compartments (Fig. 7C,D), latency difference increases with G_c and difference in input time. Dissimilar locations alter the latency modulation with a variety of effects, with synapses in varied locations shifting latency modulation curves either up (D-M) or down (M-D), producing a variety of outcomes in cell firing by as much as 20 ms. This trend is generalized in the asymmetrically conducting synapse, where G_c ratio >1 produces higher latency modulation, and values <1 shift latency modulation lower (Fig. 7B).

To examine the possible consequences of asymmetry on spike synchrony, a well noted function of electrical synapses, we used single-compartment models used previously (Haas and Landisman, 2012; Pham and Haas, 2018) to analyze correlations of tonic spike trains (Fig. 8A, B) elicited by steady current injection, with one cell (here, cell 2) driven slightly faster. Synchrony was demonstrated by peaks in steady-state cross-correlation of the spike trains (Fig. 8C,D). As electrical synapse strength increased, spike rates of the two neurons converged for coupling strength larger than 0.004 mS/cm^2 , and increased together with synapse strength because of the increase in excitability contributed by the GJ (Fig. 8E). As expected from theoretical models of coupled oscillators (Lewis and Rinzel, 2003; Saraga and Skinner, 2004), our simulations revealed synchronous firing that transitioned from stable in-phase ($\sim 0^\circ$ lag) to out-of-phase ($\sim 180^\circ$ lag) forms (Fig. 8E) for a symmetrical GJ. We next observed that asymmetry of the GJ interacted with strength and altered the form of synchrony (Fig. 8F). For weak coupling, asymmetry that increased from 0.3 to 3, altering the identity of the favored cell, brought spike times closer together and produced a transition from out-of-phase to in-

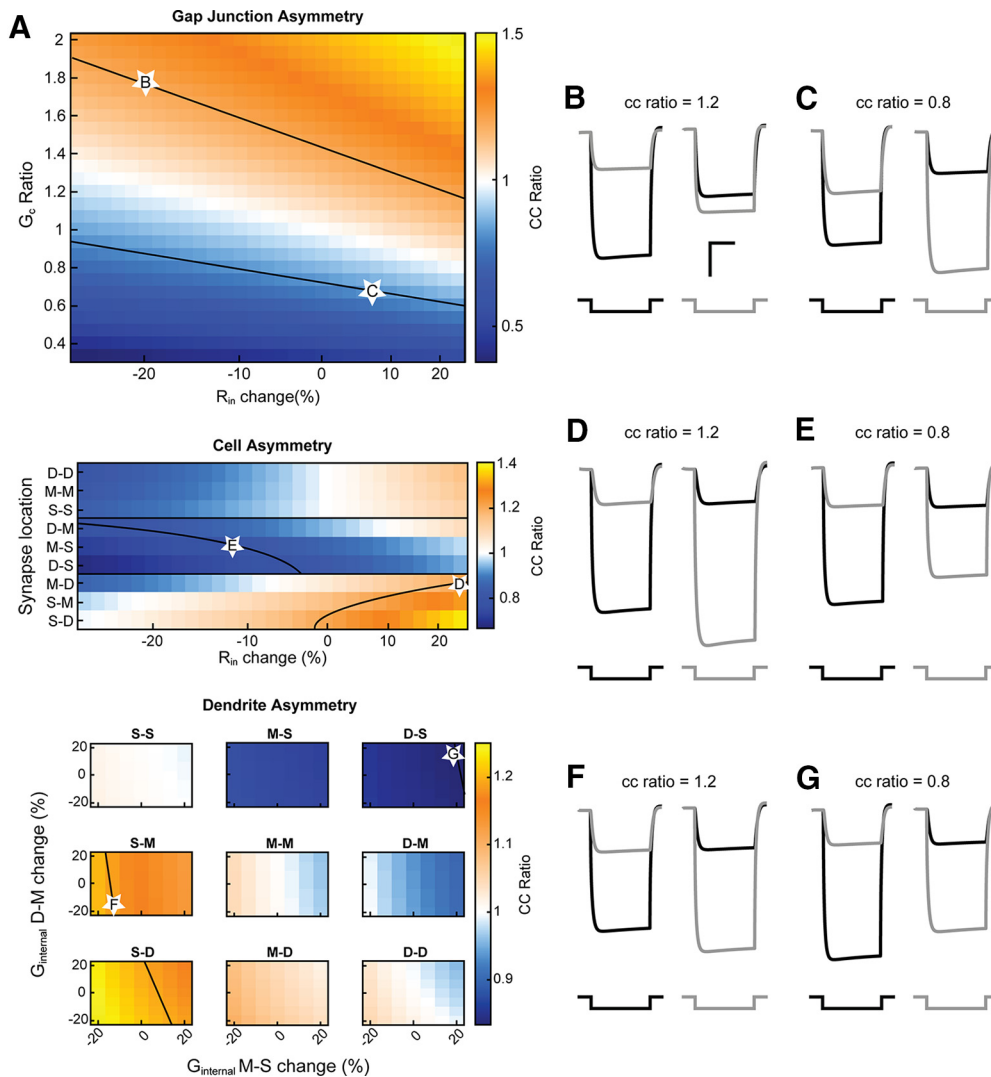


Figure 6. Varied scenarios can produce identical asymmetry as measured at the soma. **A**, Approximate isoclines (black lines) show parameters that produce the same degree of asymmetry (cc ratio of 1 ± 0.2). Representative traces (**B–G**) were taken from data along these isoclines (white stars) for cases of directionally asymmetrical conducting GJs, differing synapse locations, or differing dendritic geometries. **B**, G_C ratio 1.8, R_{in} change -20% . Scale bars: 5 mV, 200 ms. **C**, G_C ratio 0.667, R_{in} change $+6\%$. **D**, M-D GJ: R_{in} change $+25\%$. **E**, M-S GJ, R_{in} change -12% . **F**, S-M GJ, G_{MS} change -13.3% , G_{DM} change -20% . **G**, D-S GJ, G_{MS} change $+20\%$, G_{DM} change $+20\%$.

phase synchrony. The impact of asymmetry strengthened as synapse strength increased (Fig. 8F, across panels). Asymmetry that favored transmission arising from the slower cell (G_C ratio > 1) brought firing closer to in-phase, while asymmetry that favored the faster cell (G_C ratio < 1) led to out-of-phase solutions (Fig. 8G,H). These results together show that asymmetry, regardless of its subcellular source, controls synchronous rhythmic activity between coupled neurons.

Discussion

Asymmetry of transmission at electrical synapses has been widely noted but its specific sources rarely explored in depth, perhaps because of the experimental difficulties of identifying and localizing specific GJs *in vitro* or *in vivo*.

Nonetheless, because asymmetry is pervasive and can result in extreme cases in which spikes in one cell more or less faithfully drives spiking in the coupled neighbor (Apostolides and Trussell, 2013; Rash et al., 2013), we sought to understand how basic neuronal properties could influence effective coupling, and thereby the function of coupled networks. Here, we have shown that asymmetry can arise from a variety of intrinsic differences in neuronal properties as well as differences in subcellular localization of the GJ between somas. We expect additional heterogeneities, such as in the ionic currents expressed in each cell, will similarly affect coupling measurements and thus effective asymmetry, as similar activity patterns can be produced by a variety of models in pyloric circuit (Prinz et al., 2004). In practice, asymmetry is a combined product of all of these factors together. We

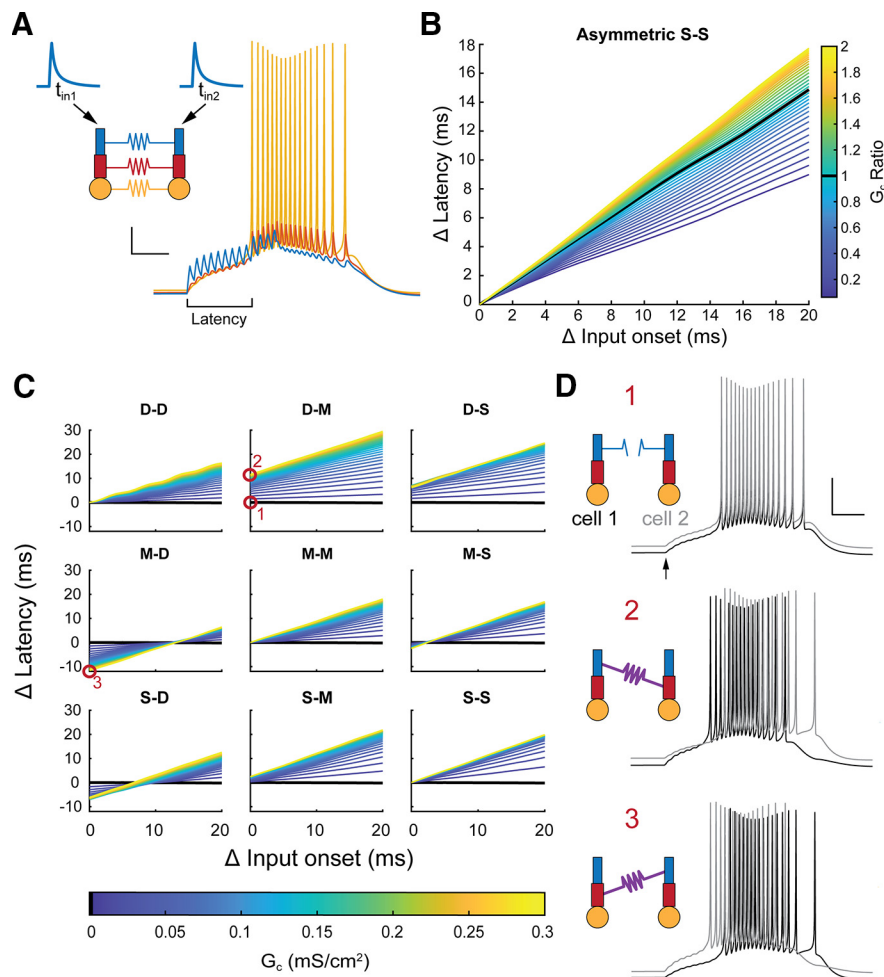


Figure 7. Asymmetry controls the latency modulation produced by electrical synapses. **A**, Each TRN cell received AMPAergic burst-like inputs (13 events with 1- μ A amplitude, 5-ms ISI) at varied onset times. Traces at right show responses of all compartments of a single cell to a burst input. Scale bars: 10 mV, 25 ms. **B**, Differences in spiking latency between the two cells plotted against difference in onset of burst inputs ($t_{in2} - t_{in1}$) for the two TRN cells. Asymmetrical somatic GJs increased GJ-mediated latency differences for G_C ratios >1 , and decreased them for G_C ratio <1 . **C**, Changes in latency for varied electrical synapse locations, strengths and input time differences. **D**, Example bursts taken from **C** (red circles) for an uncoupled pair (1), a pair with a high conductance D-M synapse (2), and high-conductance M-D synapse (3). Asymmetrical location of an electrical synapse determines bursting order, and results in positive or negative latency change. Scale bar: 20 mV, 25 ms, traces offset for clarity.

also found that asymmetrical and/or strong synapses between dendritic compartments can be masked from somatic detection by the same intrinsic properties. Our measurements here focused on soma-to-soma transmission, as ultimately, asymmetry between somas is the last stop before spike generation in the axon initial segment, and because electrical synapse strength is traditionally measured between somas. Indeed, our results also highlight that regardless of its source, asymmetry substantially impacts spike times and synchrony between coupled cells (Gutierrez and Marder, 2013; Severson and Haas, 2015).

Precise locations of electrical synapses along dendrites have proven difficult to exhaustively determine, but a handful of studies point toward asymmetrical localization. In coupled interneurons of cortex Layer IV, synapses are located all along the dendrites, and measurements from 204 cells showed strong asymmetry in localization, with

90% synapses within 50–75 μ m of one soma, but up to 250 μ m away from the coupled soma (Fukuda, 2017). Asymmetrical localization also appears to be a feature of coupling between cerebellar Golgi cells (Szoboszlay et al., 2016). The strongly asymmetrical synapses of the DCN also appear to couple mismatched distances from fusiform and stellate somas (Apostolides and Trussell, 2013). Other studies indicate that dendritic location of GJs is diverse across brain areas, and thus asymmetry could vary widely. In brainstem MesV cells, GJs appear to be located at or very close to the soma (Curti et al., 2012). In contrast, in inferior olive (Devor and Yarom, 2002; Hoge et al., 2011) cells are coupled at quite distal dendrites, such that somatic measurements of coupling themselves are small. Average intersomatic distances between coupled cells in TRN are \sim 100 μ m (Lee et al., 2014), implying that GJs are dendro-dendritic, and have a great deal of potential to create asymmetric localization of GJs between cells.

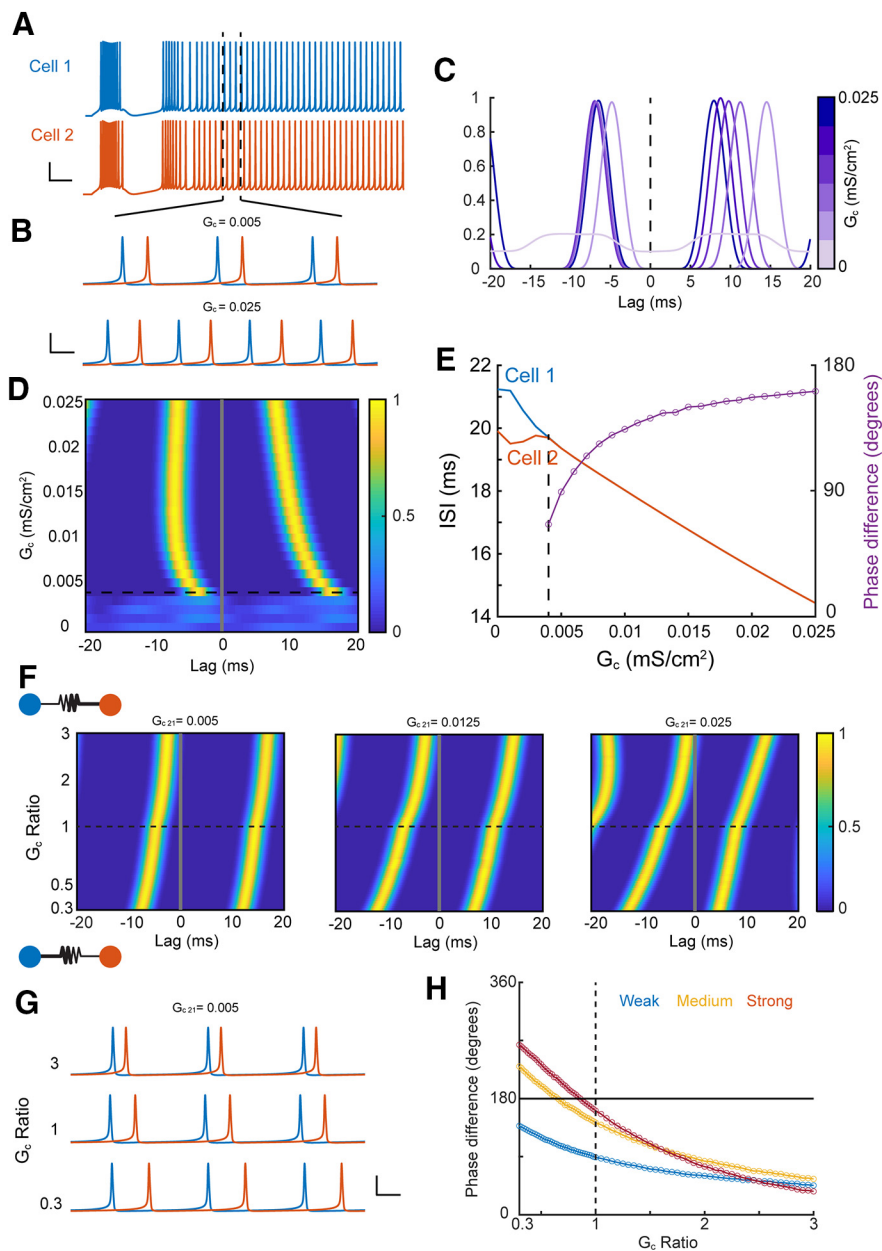


Figure 8. Asymmetry determines the phase of synchrony. **A**, Traces of two coupled TRN cells driven to spike tonically; cell 2 received a slightly larger current pulse. $I_1 = 0.575$, $I_2 = 0.6 \mu A/cm^2$. Scale bars: 25 mV, 50 ms. **B**, Zoom of tonic spikes from **A** showing synchronous firing for low coupling strength ($G_c = 0.005$ mS/cm²) and out-of-phase synchrony for higher coupling strength ($G_c = 0.025$ mS/cm²). Scale bars: 40 mV, 5 ms. **C**, Cross correlation of tonic spikes for varied values of symmetric GJ strength. **D**, Histogram of cross correlations for a symmetric synapse. **E**, ISIs for tonic spikes and phase difference (purple) of synchronous spike trains, dotted line indicates the emergence of synchrony from cross correlations in **D**. **F**, Cross correlations for asymmetric synapses. Asymmetry values >1 represent better transmission from cell 1 to cell 2. Initial strength of the GJ, $G_{c,21}$, increases across panels. **G**, Traces from weakly coupled cells in **F** for three different asymmetry conditions. Scale bars: 40 mV, 5 ms. **H**, Phase difference for asymmetric GJs from **F**, for weak (blue, $G_{c,21} = 0.005$), medium (yellow, $G_{c,21} = 0.0125$), and strong (red, $G_{c,21} = 0.025$) initial synapse strengths.

Dendritic integration is likely to be influenced by the presence of GJs along dendrites (Vervaeke et al., 2012), as they have been shown to act as a shunt of current arising from nearby chemical synapses (Linas et al., 1974; Lang et al., 1996), and in *C. elegans* coupled motor neurons, electrical synapses spread excitation during contraction and inhibit cell pairs between cycles through a

shunting effect (Choi et al., 2021). Asymmetry has also been shown to amplify EPSPs in mixed synapses (Liu et al., 2017). Additionally, dendritic morphology determines transmission across GJs (Nadim and Golowasch, 2006), as well as firing patterns of extended morphologic models (Mainen and Sejnowski, 1996), and as our results demonstrate, substantial coupling influences on

dendritic processing may not be appreciably indicated by somatic measurements.

Effective asymmetry results in differentially directed signal and information flow through a network that includes realistic electrical coupling. Our results here raise interesting questions whether cells within a network regulate any of the factors that result in asymmetry to produce precise direction of information flow within their network. Increasing electrical synapse strength through trafficking of connexin proteins, a process which is controlled by cAMP expression (Palumbos et al., 2021), may determine location or possibly effectively relocate a synapse slightly closer to or distal from the soma. Distances of dendritically located electrical synapses between cerebellar Golgi cells do not correlate with coupling strength measured between somas (Szoboszlai et al., 2016), indicating a possible compensation for distance by strength upregulation for those cells. Further, our previous work demonstrating activity-dependent plasticity showed that asymmetry changes systematically with unidirectional activity or ion flow across the GJ (Haas et al., 2011; Fricker et al., 2021). Those results imply that asymmetry is a modifiable element of electrical synapse plasticity. Our results here also point out that cellular changes, such as activity-induced changes in dendritic resistance or mutation-induced localization of GJs, could result in the changes in asymmetry measured, in addition to the possibility of changing the conductance itself.

Asymmetry, as it influences spike times in coupled cells, has downstream effects on the synaptic targets of the coupled cells. Symmetrical electrical synapses between model TRN cells act to merge spike times of thalamocortical cells in response to inputs of similar strength or timing, or can separate spikes from dissimilar inputs (Pham and Haas, 2018). We hypothesize that TRN neurons with asymmetric GJs will inhibit thalamocortical relay cells unequally, shifting the balance between merging or distinguishing signals as they are relayed to cortex. Including asymmetry as a factor in TRN networks will be important to understanding how TRN cells orchestrate the attentional spotlight at sensory thalamic nuclei. In canonical feedforward circuits, coupling between inhibitory interneurons impacts integration in principal cells (Pham and Haas, 2019). Recent investigations further show the influence of electrical synapses on temporally precise inhibition in feedforward circuits (Hoehne et al., 2020; Chagnaud et al., 2021). Asymmetry, as it can be applied to electrical synapses in these general motifs, may impact the many GJ coupled feedforward and feedback circuits that embed electrical synapses across the brain.

References

Alcami P (2018) Electrical synapses enhance and accelerate interneuron recruitment in response to coincident and sequential excitation. *Front Cell Neurosci* 12:156.

Alcami P, Marty A (2013) Estimating functional connectivity in an electrically coupled interneuron network. *Proc Natl Acad Sci USA* 110:E4798–E4807.

Amsalem O, Van Geit W, Muller E, Markram H, Segev I (2016) From neuron biophysics to orientation selectivity in electrically coupled

networks of neocortical L2/3 large basket cells. *Cereb Cortex* 26:3655–3668.

Apostolides PF, Trussell LO (2013) Regulation of interneuron excitability by gap junction coupling with principal cells. *Nat Neurosci* 16:1764–1772.

Bennett MVL (1966) Physiology of electronic junctions. *Ann NY Acad Sci* 137:509–539.

Bennett MVL, Zukin RS (2004) Electrical coupling and neuronal synchronization in the mammalian brain. *Neuron* 41:495–511.

Blatow M, Rozov A, Katona I, Hormuzdi SG, Meyer AH, Whittington MA, Caputi A, Monyer H (2003) A novel network of multipolar bursting interneurons generates theta frequency oscillations in neocortex. *Neuron* 38:805–817.

Bukauskas FF, Eifgang C, Willecke K, Weingart R (1995) Heterotypic gap junction channels (connexin26–connexin32) violate the paradigm of unitary conductance. *Pflugers Arch* 429:870–872.

Chagnaud BP, Perelmuter JT, Forlano PM, Bass AH (2021) Gap junction-mediated glycinergic inhibition ensures precise temporal patterning in vocal behavior. *Elife* 10:e59390.

Choi U, Wang H, Hu M, Kim S, Sieburth D (2021) Presynaptic coupling by electrical synapses coordinates a rhythmic behavior by synchronizing the activities of a neuron pair. *Proc Natl Acad Sci USA* 118:e2022599118.

Chow CC, Kopell N (2000) Dynamics of spiking neurons with electrical coupling. *Neural Comput* 12:1643–1678.

Christie JM, Bark C, Hormuzdi SG, Helbig I, Monyer H, Westbrook GL (2005) Connexin36 mediates spike synchrony in olfactory bulb glomeruli. *Neuron* 46:761–772.

Connelly WM, Crunelli V, Errington AC (2017) Variable action potential backpropagation during tonic firing and low-threshold spike bursts in thalamocortical but not thalamic reticular nucleus neurons. *J Neurosci* 37:5319–5333.

Curti S, Hoge G, Nagy JI, Pereda AE (2012) Synergy between electrical coupling and membrane properties promotes strong synchronization of neurons of the mesencephalic trigeminal nucleus. *J Neurosci* 32:4341–4359.

Destexhe A, Bal T, McCormick DA, Sejnowski TJ (1996) Ionic mechanisms underlying synchronized oscillations and propagating waves in a model of ferret thalamic slices. *J Neurophysiol* 76:2049–2070.

Devor A, Yarom Y (2002) Electrotonic coupling in the inferior olivary nucleus revealed by simultaneous double patch recordings. *J Neurophysiol* 87:3048–3058.

Draguhn A, Traub RD, Schmitz D, Jefferys JGR (1998) Electrical coupling underlies high-frequency oscillations in the hippocampus in vitro. *Nature* 394:189–192.

Fortier PA (2010) Detecting and estimating rectification of gap junction conductance based on simulations of dual-cell recordings from a pair and a network of coupled cells. *J Theor Biol* 265:104–114.

Fricker B, Heckman E, Cunningham PC, Wang H, Haas JS (2021) Activity-dependent long-term potentiation of electrical synapses in the mammalian thalamus. *J Neurophysiol* 125:476–488.

Fukuda T (2017) Structural organization of the dendritic reticulum linked by gap junctions in layer 4 of the visual cortex. *Neuroscience* 340:76–90.

Furshpan EJ, Potter DD (1959) Transmission at the giant motor synapses of the crayfish. *J Physiol* 145:289–325.

Galarreta M, Hestrin S (1999) A network of fast-spiking cells in the neocortex connected by electrical synapses. *Nature* 402:72–75.

Galarreta M, Hestrin S (2002) Electrical and chemical synapses among parvalbumin fast-spiking GABAergic interneurons in adult mouse neocortex. *Proc Natl Acad Sci USA* 99:12438–12443.

Gentet LJ, Ulrich D (2003) Strong, reliable and precise synaptic connections between thalamic relay cells and neurones of the nucleus reticularis in juvenile rats. *J Physiol* 546:801–811.

Gibson JR, Beierlein M, Connors BW (1999) Two networks of electrically coupled inhibitory neurons in neocortex. *Nature* 402:75–79.

- Gutierrez GJ, Marder E (2013) Rectifying electrical synapses can affect the influence of synaptic modulation on output pattern robustness. *J Neurosci* 33:13238–13248.
- Gutierrez GJ, O'Leary T, Marder E (2013) Multiple mechanisms switch an electrically coupled, synaptically inhibited neuron between competing rhythmic oscillators. *Neuron* 77:845–858.
- Haas JS (2015) A new measure for the strength of electrical synapses. *Front Cell Neurosci* 9:1–5.
- Haas JS, Landisman CE (2012) State-dependent modulation of gap junction signaling by the persistent sodium current. *Front Cell Neurosci* 5:1–13.
- Haas JS, Zavala B, Landisman CE (2011) Activity-dependent long-term depression of electrical synapses. *Science* 334:389–393.
- Hoehne A, McFadden MH, DiGregorio DA (2020) Feed-forward recruitment of electrical synapses enhances synchronous spiking in the mouse cerebellar cortex. *Elife* 9:e57344.
- Hoge GJ, Davidson KGV, Yasumura T, Castillo PE, Rash JE, Pereda AE (2011) The extent and strength of electrical coupling between inferior olivary neurons is heterogeneous. *J Neurophysiol* 105:1089–1101.
- Hormuzdi SG, Pais I, LeBeau FEN, Towers SK, Rozov A, Buhl EH, Whittington MA, Monyer H (2001) Impaired electrical signaling disrupts gamma frequency oscillations in connexin 36-deficient mice. *Neuron* 31:487–495.
- Johnson BR, Peck JH, Harris-Warrick RM (1993) Amine modulation of electrical coupling in the pyloric network of the lobster stomatogastric ganglion. *J Comp Physiol A Neuroethol Sens Neural Behav Physiol* 172:715–732.
- Kepler TB, Marder E, Abbott LF (1990) The effect of electrical coupling on the frequency of model neuronal oscillators. *Science* 248:83–85.
- Kopell N, Ermentrout B (2004) Chemical and electrical synapses perform complementary roles in the synchronization of interneuronal networks. *Proc Natl Acad Sci USA* 101:15482–15487.
- Landisman CE, Long MA, Beierlein M, Deans MR, Paul DL, Connors BW (2002) Electrical synapses in the thalamic reticular nucleus. *J Neurosci* 22:1002–1009.
- Lang EJ, Sugihara I, Llinas R (1996) GABAergic modulation of complex spike activity by the cerebellar nucleoolivary pathway in rat. *J Neurophysiol* 76:21.
- Lee SC, Patrick SL, Richardson KA, Connors BW (2014) Two functionally distinct networks of gap junction-coupled inhibitory neurons in the thalamic reticular nucleus. *J Neurosci* 34:13170–13182.
- Lewis TJ, Rinzel J (2003) Dynamics of spiking neurons connected by both inhibitory and electrical coupling. *J Comp Neurosci* 14:283–309.
- Li X, Olson C, Lu S, Kamasawa N, Yasumura T, Rash JE, Nagy JI (2004) Neuronal connexin36 association with zonula occludens-1 protein (ZO-1) in mouse brain and interaction with the first PDZ domain of ZO-1. *Eur J Neurosci* 19:2132–2146.
- Liu P, Chen B, Mailler R, Wang Z-W (2017) Antidromic-rectifying gap junctions amplify chemical transmission at functionally mixed electrical-chemical synapses. *Nat Commun* 8:14818.
- Llinas R, Baker R, Sotelo C (1974) Electrotonic coupling between neurons in cat inferior olive. *J Neurophysiol* 37:560–571.
- Long MA, Landisman CE, Connors BW (2004) Small clusters of electrically coupled neurons generate synchronous rhythms in the thalamic reticular nucleus. *J Neurosci* 24:341–349.
- Long MA, Jutras MJ, Connors BW, Burwell RD (2005) Electrical synapses coordinate activity in the suprachiasmatic nucleus. *Nat Neurosci* 8:61–66.
- Mainen ZF, Sejnowski TJ (1996) Influence of dendritic structure on firing pattern in model neocortical neurons. *Nature* 382:363–366.
- Mamiya A, Manor Y, Nadim F (2003) Short-term dynamics of a mixed chemical and electrical synapse in a rhythmic network. *J Neurosci* 23:9557–9564.
- Mann-Metzer P, Yarom Y (1999) Electrotonic coupling interacts with intrinsic properties to generate synchronized activity in cerebellar networks of inhibitory interneurons. *J Neurosci* 19:3298–3306.
- Manor Y, Rinzel J, Segev I, Yarom Y (1997) Low-amplitude oscillations in the inferior olive: a model based on electrical coupling of neurons with heterogeneous channel densities. *J Neurophysiol* 77:2736–2752.
- Marder E (1998) Electrical synapses: beyond speed and synchrony to computation. *Curr Biol* 8:R795–R797.
- Marsh AJ, Michel JC, Adke AP, Heckman EL, Miller AC (2017) Asymmetry of an intracellular scaffold at vertebrate electrical synapses. *Curr Biol* 27:3561–3567.e4.
- Nadim F, Golowasch J (2006) Signal transmission between gap-junctionally coupled passive cables is most effective at an optimal diameter. *J Neurophysiol* 95:3831–3843.
- Nomura M, Aoyagi T, Fukai T (2004) Gamma frequency synchronization in a local cortical network model. *Neurocomputing* 58–60:173–178.
- O'Connor S, Angelo K, Jacob TJC (2012) Burst firing versus synchrony in a gap junction connected olfactory bulb mitral cell network model. *Front Comput Neurosci* 6:75.
- Palacios-Prado N, Hoge G, Marandykina A, Rimkute L, Chapuis S, Paulauskas N, Skeberdis VA, O'Brien J, Pereda AE, Bennett MVL, Bukauskas FF (2013) Intracellular magnesium-dependent modulation of gap junction channels formed by neuronal connexin36. *J Neurosci* 33:4741–4753.
- Palumbos SD, Skelton R, McWhirter R, Mitchell A, Swann I, Heifner S, Von Stetina S, Miller DM (2021) cAMP controls a trafficking mechanism that maintains the neuron specificity and subcellular placement of electrical synapses. *Dev Cell* 56:3235–3249.e4.
- Pernelle G, Nicola W, Clopath C (2018) Gap junction plasticity as a mechanism to regulate network-wide oscillations. *PLoS Comput Biol* 14:e1006025.
- Pfeuty B, Mato G, Golomb D, Hansel D (2005) The combined effects of inhibitory and electrical synapses in synchrony. *Neural Comput* 17:633–670.
- Pham T, Haas JS (2018) Electrical synapses between inhibitory neurons shape the responses of principal neurons to transient inputs in the thalamus: a modeling study. *Sci Rep* 8:7763.
- Pham T, Haas JS (2019) Electrical synapses regulate both subthreshold integration and population activity of principal cells in response to transient inputs within canonical feedforward circuits. *PLoS Comput Biol* 15:e1006440.
- Phelan P, Goulding LA, Tam JLY, Allen MJ, Dawber RJ, Davies JA, Bacon JP (2008) Molecular mechanism of rectification at identified electrical synapses in the *Drosophila* giant fiber system. *Curr Biol* 18:1955–1960.
- Prinz AA, Bucher D, Marder E (2004) Similar network activity from disparate circuit parameters. *Nat Neurosci* 7:1345–1352.
- Rash JE, Curti S, Vanderpool KG, Kamasawa N, Nannapaneni S, Palacios-Prado N, Flores CE, Yasumura T, O'Brien J, Lynn BD, Bukauskas FF, Nagy JI, Pereda AE (2013) Molecular and functional asymmetry at a vertebrate electrical synapse. *Neuron* 79:957–969.
- Saraga F, Skinner FK (2004) Location, location, location (and density) of gap junctions in multi-compartment models. *Neurocomputing* 58–60:713–719.
- Sevetson J, Haas JS (2015) Asymmetry and modulation of spike timing in electrically coupled neurons. *J Neurophysiol* 113:1743–1751.
- Sherman A, Rinzel J (1992) Rhythmogenic effects of weak electrotonic coupling in neuronal models. *Proc Natl Acad Sci USA* 89:2471–2474.
- Shui Y, Liu P, Zhan H, Chen B, Wang Z-W (2020) Molecular basis of junctional current rectification at an electrical synapse. *Sci Adv* 6:eabb3076.
- Skinner FK, Zhang L, Velazquez JLP, Carlen PL (1999) Bursting in inhibitory interneuronal networks: a role for gap-junctional coupling. *J Neurophysiol* 81:1274–1283.
- Snipas M, Rimkute L, Kraujalis T, Maciunas K, Bukauskas FF (2017) Functional asymmetry and plasticity of electrical synapses interconnecting neurons through a 36-state model of gap junction channel gating. *PLoS Comput Biol* 13:e1005464.

- Srinivas M, Rozental R, Kojima T, Dermietzel R, Mehler M, Condorelli DF, Kessler JA, Spray DC (1999) Functional properties of channels formed by the neuronal gap junction protein connexin36. *J Neurosci* 19:9848–9855.
- Szoboszlay M, Lőrincz A, Lanore F, Vervaeke K, Silver RA, Nusser Z (2016) Functional properties of dendritic gap junctions in cerebellar golgi cells. *Neuron* 90:1043–1056.
- Tamás G, Buhl EH, Lőrincz A, Somogyi P (2000) Proximally targeted GABAergic synapses and gap junctions synchronize cortical interneurons. *Nat Neurosci* 3:366–371.
- Teubner B, Degen J, Söhl G, Güldenagel M, Bukauskas FF, Trexler EB, Verselis VK, De Zeeuw CI, Lee CG, Kozak CA, Petrasch-Parwez E, Dermietzel R, Willecke K (2000) Functional expression of the murine connexin 36 gene coding for a neuron-specific gap junctional protein. *J Membr Biol* 176:249–262.
- Traub RD, Contreras D, Cunningham MO, Murray H, LeBeau FEN, Roopun A, Bibbig A, Wilentz WB, Higley MJ, Whittington MA (2005) Single-column thalamocortical network model exhibiting gamma oscillations, sleep spindles, and epileptogenic bursts. *J Neurophysiol* 93:2194–2232.
- Veruki ML, Hartveit E (2002) All (rod) amacrine cells form a network of electrically coupled interneurons in the mammalian retina. *Neuron* 33:935–946.
- Vervaeke K, Lorincz A, Gleeson P, Farinella M, Nusser Z, Silver RA (2010) Rapid desynchronization of an electrically coupled interneuron network with sparse excitatory synaptic input. *Neuron* 67:435–451.
- Vervaeke K, Lorincz A, Nusser Z, Silver RA (2012) Gap junctions compensate for sublinear dendritic integration in an inhibitory network. *Science* 335:1624–1628.
- Whittington MA, Traub RD (2003) Interneuron diversity series: inhibitory interneurons and network oscillations in vitro. *Trends Neurosci* 26:676–682.
- Zolnik TA, Connors BW (2016) Electrical synapses and the development of inhibitory circuits in the thalamus: electrical synapses and thalamic development. *J Physiol* 594:2579–2592.